

Classical analysis of phase-locking transients and Rabi-type oscillations in microwave-driven Josephson junctions

Jeffrey E. Marchese

Department of Applied Science, University of California, Davis, California 95616

Matteo Cirillo

Dipartimento di Fisica and INFN, Università di Roma "Tor Vergata", I-00173 Roma, Italy

Niels Grønbech-Jensen

Department of Applied Science, University of California, Davis, California 95616

(Dated: May 6, 2019)

Abstract

We present a classical analysis of the transient response of Josephson junctions perturbed by microwaves and thermal fluctuations. The results include a specific low frequency modulation in phase and amplitude behavior of a junction in its zero-voltage state. This transient modulation frequency is linked directly to an observed variation in the probability for the system to switch to its non-zero voltage state. Complementing previous work on linking classical analysis to the experimental observations of Rabi-oscillations, this expanded perturbation method also provides closed form analytical results for attenuation of the modulations and the Rabi-type oscillation frequency. Results of perturbation analysis are compared directly (and quantitatively) to numerical simulations of the classical model as well as published experimental data, suggesting that transients to phase-locking are closely related to the observed oscillations.

PACS numbers: 74.50.+r,03.67.Lx,85.25.Cp

I. INTRODUCTION

Much experimental attention has recently been given to the topic of Rabi-oscillations [1] in microwave irradiated Josephson systems at very low temperatures [2, 3, 4, 5]. A common motivation for the studies is the proposed macroscopic quantum behavior outlined in Ref. [6], which has opened the way for potential applications of Josephson technology in quantum information processing [7]. This is proposed by operating a Josephson junction in its zero-voltage state at temperatures below the quantum transition temperature, while manipulating the possible energy states with the application of commensurate microwave frequencies. The significance of Rabi-oscillations is many fold, and includes *i*) a direct connection to a well known quantum mechanical concept in perturbed atomic systems, and *ii*) a method by which the control of quantum states of a system can be evaluated. Thus, it is of significant importance to understand the nature of these observations in order for us to evaluate how to interpret the Josephson system under investigation.

Recent classical analyses of Josephson junctions, perturbed by microwaves and low temperature thermal fluctuations, have revealed that key signatures of microwave-induced multi-peaked switching distributions [8, 9, 10, 11], used to display quantum mechanical features of Josephson junctions, have direct classical analogs, which may obscure the interpretation of the observations [12, 13, 14, 15]. Inspired by the work on slowly modulated transients to phase-locking in Josephson systems by Lomdahl and Samuelsen [16], it has most recently been demonstrated [17] that also Rabi-oscillations have a classical analogue in microwave perturbed Josephson junctions, providing a system response very similar to reported observations under the same conditions. We therefore denote this classical phenomenon Rabi-type oscillations. It is the aim of this paper to complement and expand on the analysis provided in Ref. [17] in order to extract more detailed information from the classical model as it relates to observations of Rabi-oscillations. We further demonstrate the validity of the analysis through direct quantitative comparisons with the observations of Ref. [5], in which enough information is provided to conduct direct quantitative comparisons with our theory. Specifically, we present an analysis based on direct perturbations in the dynamical variables. This approach results in closed form results that include dissipation, which is of direct importance for experimental measurements of, e.g, coherence time.

We will start section II by providing the system equations that govern the classical model

as it relates to specific reported measurements of Rabi-oscillations. Next, in section III, we present a new, more complete, perturbation analysis of the slow transient modulations to phase-locking, and provide specific analytical results for (Rabi) oscillation frequency and attenuation as a function of the system parameters. The theory is numerically validated in section IV. Direct observations of Rabi-type oscillations in the classical model are produced in section V through numerical simulations of a system parameterized to mimic reported experiments, and close agreement is found between these simulations, the developed theory, and the reported experiments. We conclude the paper in section VI.

II. CLASSICAL MODEL

A normalized classical equation for a Josephson junction can be written [18]

$$\ddot{\varphi} + \alpha\dot{\varphi} + \sin \varphi = \eta + \varepsilon_s(t) \sin(\omega_s t + \theta_s) + \varepsilon_p(t) + n(t) , \quad (1)$$

where φ is the difference between the phases of the quantum mechanical wave functions defining the junction, η represents the dc bias current, and $\varepsilon_s(t)$ and ω_s represent microwave current amplitude and frequency, respectively. All currents are normalized to the critical current I_c , and time is measured in units of the inverse plasma frequency ω_0^{-1} , where $\omega_0^2 = 2eI_c/\hbar C = 2\pi I_c/\Phi_0 C$, C being the capacitance of the junction and $\Phi_0 = h/2e$ the flux quantum. The phase of the applied microwave field is θ_s . Tunneling of quasiparticles is represented by the dissipative term, where $\alpha = \hbar\omega_0/2eRI_c$ is given by the shunt resistance R , and the accompanying thermal fluctuations are defined by the dissipation-fluctuation relationship [19]

$$\langle n(t) \rangle = 0 \quad (2)$$

$$\langle n(t)n(t') \rangle = 2\alpha \frac{k_B T}{H_J} \delta(t - t') , \quad (3)$$

T being the temperature and $H_J = I_c\Phi_0/2\pi$ is the characteristic Josephson energy. A current pulse for probing the state of the system is represented by $\varepsilon_p(t)$.

From the above normalizations, we define the normalized energy from the time independent perturbation terms in Equation (1)

$$H = \frac{1}{2}\dot{\varphi}^2 + 1 - \cos \varphi - \eta\varphi . \quad (4)$$

The undamped bias current dependent plasma frequency is given by

$$\omega_J = \sqrt[4]{1 - \eta^2}. \quad (5)$$

Within this model, we will make analysis and conduct simulations according to experiments reported in Ref. [5]. System parameters, such as η , α , ω_s , $\varepsilon_s(t)$, and $\varepsilon_p(t)$ are matched as closely as possible to reported values, and Rabi-type oscillations are observed statistically through simulations of the distribution of probe field induced switching from the zero-voltage state as a function of applied microwave field $\varepsilon_s(t) \sin(\omega_s t + \theta_s)$. Microwave and probe perturbations have the form sketched in Figure 1. We assume the phase θ_s of the microwave field is random for each switching event. Notice the difference in probe field between this presentation (along with Ref. [5]) compared to Refs. [2, 4, 17], where the probe was a microwave field with frequency slightly lower than ω_s .

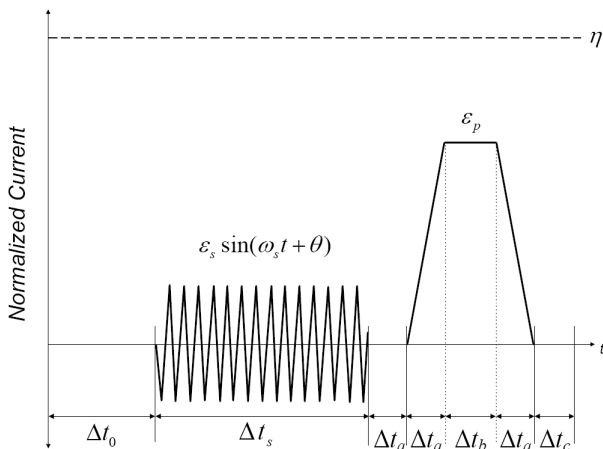


FIG. 1: Schematic of signaling protocol, which is adopted from Ref. [5]. Dotted line represents the dc bias η which is constant throughout each run. The normalized time interval Δt_0 represents a 91 ns duration during which no ac signal is present to allow the junction to achieve a steady-state. Δt_s represents the duration of the ac signal. This value is varied so as to observe the temporal Rabi-type oscillations. Values for the signal timings are $\Delta t_a = 1.5ns\omega_0$, $\Delta t_b = 2.5ns\omega_0$, and $\Delta t_c = 2.0ns\omega_0$.

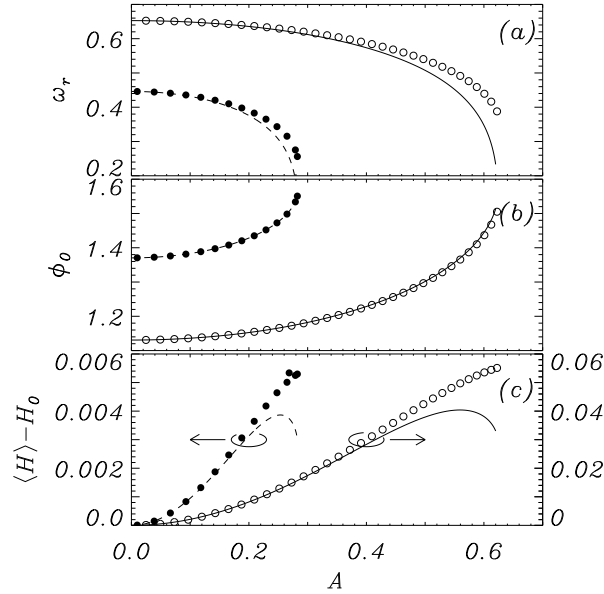


FIG. 2: Comparison between numerical results of Equation (1) (markers) and the monochromatic ansatz Equation (6) (curves) for $\alpha = \varepsilon_s(t) = \varepsilon_p(t) = T = 0$. Results for $\eta = 0.904607$ are displayed with \circ and solid curves, while results for $\eta = 0.98$ are displayed with \bullet and dashed curves. (a) Anharmonic relationship between amplitude A and frequency ω_r Equation (8); (b) amplitude A and average phase φ_0 Equation (7); and (c) amplitude A and normalized energy $H - H_0$ Equations (9) and (10).

III. PERTURBATION ANALYSIS

Following the analysis of Refs. [13, 14, 20], we will use the monochromatic ansatz for a solution of the unperturbed Equation (1) ($\alpha = \varepsilon_s(t) = T = \varepsilon_p(t) = 0$)

$$\varphi = \varphi_0 + \psi = \varphi_0 + A \sin(\omega t + \theta), \quad (6)$$

where φ_0 is the average phase, A is an oscillation amplitude (which is not necessarily small), and ω is the natural frequency. Inserting this ansatz into Equation (1), we obtain the anharmonic relationships between the parameters

$$J_0(A) \sin \varphi_0 = \eta \quad (7)$$

$$\omega^2 = \omega_r^2 = \frac{2J_1(A)}{A} \sqrt{1 - \left(\frac{\eta}{J_0(A)}\right)^2}, \quad (8)$$

where J_n is the n th order Bessel function of the first kind [21]. Notice that the ansatz dictates $J_0(A) > \eta$ as a condition for existence of a zero-voltage state. Also notice that

$\omega_r \leq \omega_J$ and that $\omega_r \rightarrow \omega_J$ for $A \rightarrow 0$. The average system energy of the monochromatic ansatz is found by inserting Equations (6) and (7) into (4), then average over the period given by (8),

$$\langle H \rangle_{\frac{2\pi}{\omega}} = \frac{1}{4}A^2\omega^2 + 1 - J_0(A) \cos \varphi_0 - \eta\varphi_0, \quad (9)$$

where the minimum energy H_0 for a given η is

$$H_0 = 1 - \sqrt{1 - \eta^2} - \eta \sin^{-1}\eta. \quad (10)$$

The applicability of this very simple monochromatic ansatz (6) is illustrated in Figure 2. Here we have shown the average phase φ_0 and oscillation frequency ω_r as a function of oscillation amplitude A for two different values of dc bias η . Data are obtained from direct numerical simulations of Equation (1) (markers) and from Equations (7)-(10) (curves). The agreement between the results of the ansatz and the simulations is very close, except at the highest amplitudes (when $J_0(A) \rightarrow \eta$), where higher harmonics of the dynamics contribute significant components to the dynamics. We use this ansatz to develop a perturbation theory for the system response to the application of microwaves and damping.

For $T = \varepsilon_p(t) = 0$ we now separate the parameters of the ansatz into steady state and small time dependent deviations; $A = \bar{A} + \delta A$, $\theta = \bar{\theta} + \delta\theta$, and $\varphi = \bar{\varphi}_0 + \delta\varphi_0$, where $|\delta A| \ll 1$, $|\delta\theta| \ll 1$, and $|\delta\varphi_0| \ll 1$. Inserting Equation (6) into (1) for $\varepsilon_p(t) = T = 0$ and $\varepsilon_s(t) = \Theta(t)\varepsilon_s$ (Θ being Heavyside's step function), yields the steady state phase-locked relationships [13, 17]

$$\varepsilon_s^2 = \bar{A}^2 \left((\omega_s^2 - \omega_r^2)^2 + \alpha^2 \omega_s^2 \right) \quad (11)$$

$$\tan(\bar{\theta} - \theta_s) = \frac{\alpha \omega_s}{\omega_s^2 - \omega_r^2}, \quad (12)$$

and the linearized expressions for the small deviations from steady state:

$$\delta\ddot{\varphi}_0 + \alpha\dot{\delta\varphi}_0 + J_0(\bar{A}) \cos \bar{\varphi}_0 \delta\varphi_0 = J_1(\bar{A}) \sin \bar{\varphi}_0 \delta A \quad (13)$$

$$\delta\ddot{A} + \alpha(\dot{\delta A} - \omega_s \bar{A} \delta\theta) - 2\omega_s \bar{A} \dot{\delta\theta} + \left[(J_0(\bar{A}) - J_2(\bar{A})) \cos \bar{\varphi}_0 - \omega_s^2 \right] \delta A = 2J_1(\bar{A}) \sin \bar{\varphi}_0 \delta\varphi_0 \quad (14)$$

$$\bar{A} \delta\ddot{\theta} + \alpha(\bar{A} \dot{\delta\theta} + \omega_s \delta A) + 2\omega_s \dot{\delta A} + \left[(J_0(\bar{A}) + J_2(\bar{A})) \cos \bar{\varphi}_0 - \omega_s^2 \right] \bar{A} \delta\theta = 0. \quad (15)$$

Equation (13) represents the small amplitude, slowly varying terms in (1), while (14) and (15) represent small amplitude terms oscillating with ω_s . Evaluating a solution to Equations (13)-(15) is not simple, but making the assumption that all three variables oscillate slowly with

the same frequency Ω_R and decay with the same attenuation β , we can write the simple relationships: $\delta A = \exp(i\Omega t)$, $\bar{A}\delta\theta = \kappa\delta A$, and $\delta\varphi_0 = \gamma\delta A$, with $\Omega = \Omega_R + i\beta$. This results in the following polynomial

$$\begin{aligned} & \Omega^6 - 3i\alpha\Omega^5 - \left[\frac{15}{4}\alpha^2 - a_4\right]\Omega^4 + i\alpha\left[\frac{5}{2}\alpha^2 - 2a_4\right]\Omega^3 + \left[\frac{15}{16}\alpha^4 - \frac{3}{2}\alpha^2 a_4 + a_2\right]\Omega^2 \\ & - i\alpha\left[\omega_s^2\alpha^2 + \Gamma_1\right]\Omega = \alpha^2\omega_s^2 J_0(\bar{A})\cos\bar{\varphi}_0 + \Gamma_2, \end{aligned} \quad (16)$$

where the parameters a_i and Γ_i are given in Equations (18)-(22) below. The polynomial can be simplified considerably by inserting $\Omega = \Omega_R + i\beta$, and realizing that $\beta = \frac{1}{2}\alpha$ is the complex part of the roots (for all roots) with a non-zero real part Ω_R ; i.e., for underdamped modulations. Notice that dissipative systems ($\alpha > 0$) will naturally imply that $\Omega_R^2 \rightarrow 0_+$ for a nonzero threshold value of the microwave amplitude $\varepsilon_s > 0$ [16, 17]. With $\beta = \frac{1}{2}\alpha$ the (real) modulation frequency Ω_R is determined by the following real polynomial:

$$\Omega_R^6 + a_4\Omega_R^4 + a_2\Omega_R^2 + a_0 = 0, \quad (17)$$

where

$$a_4 = \frac{3}{4}\alpha^2 - 2\omega_s^2 - 3J_0(\bar{A})\cos\bar{\varphi}_0 \quad (18)$$

$$a_2 = \frac{3}{16}\alpha^4 - \frac{3}{2}\alpha^2 J_0(\bar{A})\cos\bar{\varphi}_0 + \Gamma_1 \quad (19)$$

$$a_0 = \frac{1}{64}\alpha^6 - \frac{1}{16}\alpha^4 a_4 + \alpha^2\left(\frac{a_2}{4} - \omega_s^2 J_0(\bar{A})\cos\bar{\varphi}_0\right) - \Gamma_2 \quad (20)$$

$$\begin{aligned} \Gamma_1 = & (\omega_s^2 - \bar{\omega}_r^2)\left(\omega_s^2 + \bar{\omega}_r^2 - 2J_0(\bar{A})\cos\bar{\varphi}_0\right) + 2\left(J_0(\bar{A})\cos\bar{\varphi}_0 + \omega_s^2\right)J_0(\bar{A})\cos\bar{\varphi}_0 \\ & - 2J_1^2(\bar{A})\sin^2\bar{\varphi}_0 \end{aligned} \quad (21)$$

$$\Gamma_2 = (\omega_s^2 - \bar{\omega}_r^2)\left[\left(\omega_s^2 + \bar{\omega}_r^2 - 2J_0(\bar{A})\cos\bar{\varphi}_0\right)J_0(\bar{A})\cos\bar{\varphi}_0 + 2J_1^2(\bar{A})\sin^2\bar{\varphi}_0\right]. \quad (22)$$

The steady-state resonance frequency $\bar{\omega}_r$ is given by Equation (8) as a function of \bar{A} . Generally speaking, the three roots Ω_R^2 are real and positive. One is located near $(2\omega_s)^2$, one near ω_s^2 , and one much smaller than ω_s^2 . It is the latter we are interested in when studying transients and modulations to phase-locking, and it can be very well approximated by either of the following approximations, since the normalized frequency is small:

$$\Omega_R^2 \approx -\frac{a_0}{a_2} \quad (23)$$

$$\Omega_R^2 \approx \frac{-a_2 + \sqrt{a_2^2 - 4a_0a_4}}{2a_4} \quad (24)$$

A further simplification to the coefficients in the polynomial can be produced by noticing that the damping parameter α in relevant Josephson experiments is very small, allowing for omission of several terms of high order in α in Equations (18)-(20). A specific limit of the above solution can be derived for small oscillation (A) and microwave (ε_s) amplitudes for $\alpha = 0$ and $\omega_s^4 \equiv 1 - \eta^2$

$$\Omega_R \approx \sqrt{\frac{\Gamma_2}{\Gamma_1}} \quad (25)$$

$$\rightarrow \bar{A}^2 \frac{\sqrt{3}}{16} \frac{2 - \omega_s^4}{\omega_s^3} = \bar{A}^2 \frac{\sqrt{3}}{16} \frac{1 + \eta^2}{(1 - \eta^2)^{\frac{3}{4}}}, \text{ for } A \rightarrow 0 \quad (26)$$

$$= \varepsilon_s^{\frac{2}{3}} \frac{\sqrt{3}}{4} \frac{(2 - \omega_s^4)^{\frac{1}{3}}}{\omega_s^{\frac{5}{3}}} = \varepsilon_s^{\frac{2}{3}} \frac{\sqrt{3}}{4} \frac{(1 + \eta^2)^{\frac{1}{3}}}{(1 - \eta^2)\omega_s^{\frac{5}{12}}}, \text{ for } \varepsilon_s \rightarrow 0. \quad (27)$$

The resonant choice $\omega_s^4 \approx 1 - \eta^2$ is consistent with the experimental studies [5]. In fact, measurements are usually conducted for ω_s very close to the linear resonance frequency (see, e.g., Ref. [2, 4]). However, if $\omega_s^4 \neq 1 - \eta^2$, then $A \propto \varepsilon_s$, and the relationship between Ω_R^2 and ε_s^2 becomes linear for small values of A and ε_s . Further, if $\omega_s^4 \lesssim 1 - \eta^2$, A may become a multi-valued function of ε_s , corresponding to several resonant energy states of the system for the same parameter values [17].

The solution to Equation (17), which can be given in closed form as a solution to a third order polynomial, is a complementary, more convenient, approach to the one presented in Ref. [17]. It provides the important additional information regarding the attenuation β of the transient modulations and it provides explicit expressions for the modulation frequency as a function of all system parameters. The two different perturbation methods agree qualitatively, and are quantitatively similar. The main difference between the two approaches is that we have here considered phase θ and amplitude A as harmonically varying variables, instead of using the energy balance approach to transients [16], which treats the total energy of the system as the linearized dynamical variable. Notice that the linearized Equations (13)-(15) provide information about frequency, attenuation, and internal phase-relationships, but not about the specific magnitude of the deviations. However, the magnitude can be quantitatively estimated from the following reasoning. For a simulation, in which a Josephson junction is described by Equation (1) with $\varepsilon_p(t) = T = 0$ (or at least very low temperature) and $\varepsilon_s(t) = \Theta(t)\varepsilon_s$, the system is at rest $\varphi = \varphi_0 = \sin^{-1}\eta$ for $t < 0$ ($A = 0$). The onset of the microwave field at $t = 0$ will therefore, within the harmonic approximation, produce an

envelope function of oscillation given by [22]

$$A = \bar{A} + \delta A = \begin{cases} 0 & , t \leq 0 \\ \bar{A} \left(1 - e^{-\beta t} \cos \Omega_R t\right) & , t > 0 \end{cases} . \quad (28)$$

The two other modulated variables, $\delta\varphi_0 = \gamma\delta A$ and $\bar{A}\delta\theta = \kappa\delta A$, can then be found from the coefficients

$$\gamma = \frac{-J_1(\bar{A}) \sin \bar{\varphi}_0}{\Omega^2 - i\alpha\Omega - J_0(\bar{A}) \cos \bar{\varphi}_0} \quad (29)$$

$$\kappa = \frac{\alpha\omega_s + 2i\omega_s\Omega}{\Omega^2 - i\alpha\Omega + \omega_s^2 - \omega_r^2} . \quad (30)$$

The modulated system energy (for $\varepsilon_p(t) = 0$) can be calculated from Equation (9) as

$$\langle H \rangle_{\frac{2\pi}{\omega_s}} = \bar{H} + \delta H , \quad (31)$$

where \bar{H} is the steady state energy of the phase-locked state in Equations (11) and (12), and δH is the transient modulation. The average phase φ_0 can be calculated either as a function of $A = \bar{A} + \delta A$ as given by Equations (7) and (28), or it can be extracted from the theory through Equation (29). The two results are very similar, but since the latter is a first order approximation in the perturbation theory, it will have a second order error at $t = 0$. Using Equation (7), $\varphi_0(t)$ will satisfy the true value both at $t = 0$ and for $t \rightarrow \infty$.

IV. SIMULATION OF TRANSIENTS

Numerical validation of the expressions for the transient modulation can be directly acquired from simulating Equation (1) for $\varepsilon_p(t) = T = 0$ and $\varepsilon_s(t) = \varepsilon_s\Theta(t)$ for different values of $\omega_s^4 = 1 - \eta^2$ and α . Simulations are conducted by choosing $\eta < 1$ and $\alpha \geq 0$, then initiating the system in the static state $(\varphi(0), \dot{\varphi}(0)) = (\sin^{-1}\eta, 0)$. At $t = 0$, the microwave field switches on, and we measure the phase $\varphi(t)$, the average phase $\varphi_0(t) = \langle \varphi(t) \rangle_{\frac{2\pi}{\omega_s}}$, and the system energy $H(t)$ as given by Equation (4). Figure 3 shows a typical comparison between the analysis of the previous section and direct numerical simulations. We have chosen system parameters $\alpha = 0.00151477$, $\eta = 0.904706$, $\varepsilon_s = 0.00108 \cdot \Theta(t)$, and $\omega_s = \sqrt[4]{1 - \eta^2} = 0.6527147$ (inspired by Ref. [5]). We can clearly see that the transient in phase and amplitude is a very slow modulation, and that this modulation provides a slow transient oscillation in the system energy. Notice that the phase-locked frequency is *much*

higher than the depicted modulation, $\Omega_R \ll \omega_s$. We have shown results of the theory on the left (Figures 3a and b) and the corresponding simulation results on the right (Figures 3c and d). The quantitative agreement between the results is obvious. We do see a slightly larger predicted oscillation amplitude compared to the simulated. We also notice a slightly higher predicted modulation frequency than what is observed in the simulations. Despite these slight discrepancies, which are usually about 5% and no larger than about 10%, we consider this remarkable agreement given the simple monochromatic trial function and the linearization in the perturbation treatment. Figure 4 shows the details of the perturbation variables as calculated from the theory, and they reveal that the actual oscillation frequency $\omega = \omega_s + \dot{\delta}\theta$ is only insignificantly different from ω_s . Direct comparisons between the predicted modulation Ω and the simulated values as a function of microwave amplitude for different values of η and α are summarized in Figures 5 and 6. Comparisons for Ω_R are provided in Figure 5 and the attenuation β is validated in Figure 6. The general agreement is very good for all parameters tested. We observe the simple relationship $\beta = \alpha/2$ for all oscillating solutions and the general trend of the polynomial (Equation (16) or (17)) is to provide a modulation frequency slightly larger than what is observed in simulations. This is quantitatively similar to the values obtained from the energy balance perturbation theory developed in Ref. [17], where the true modulation frequency was consistently slightly under-estimated. We finally observe the broad applicability of the asymptotic value of the modulation frequency given in Equation (27).

V. RABI-TYPE OSCILLATIONS

As was argued in Ref. [17], the Rabi-oscillations observed in, e.g., Refs. [2, 4, 5] may be closely related to the classical transient modulations described above. The numerical simulations in Ref. [17] were conducted in close agreement with the procedures described in Ref. [2], by applying a small temperature $T \approx 50mK$ ($kT/H_J \sim 10^{-2} \ll 1$) to a Josephson junction, which is perturbed by a microwave pulse starting at $t = 0$ with a frequency $\omega_s = \sqrt[4]{1 - \eta^2}$. Varying either the microwave amplitude or duration may yield Rabi-type oscillations in switching probability when a subsequent microwave pulse with a smaller frequency $\omega_p < \omega_s$ is applied to probe the energy state of the junction as it is left by the first microwave pulse. The frequency of the second (probe) field was chosen to match an

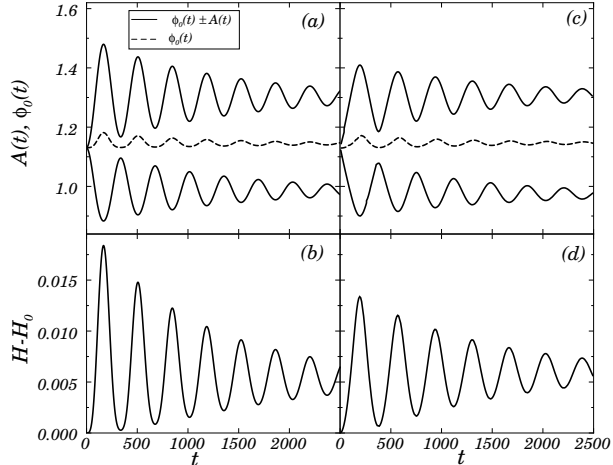


FIG. 3: Normalized time response in phase amplitude A and average phase φ_0 (a and c) and normalized energy $H - H_0$ (b and d) as a function of time after onset of microwave perturbation. Figures a and b show results of the perturbation theory Equations (7)-(11) and (28). Figures c and d show results of direct simulations of Equation (1) for the same parameters as (a and b). Parameters are: $\alpha = 0.00151477$, $\eta = \sqrt{1 - \omega_s^4} = 0.904706$, $\varepsilon_s(t) = 0.00108 \cdot \Theta(t)$, and $T = \varepsilon_p(t) = 0$.

anharmonic amplitude that could excite the junction beyond the energy saddle point and lead to escape from the well. The measurements were conducted for varying microwave amplitude and fixed microwave duration.

The experiments described in Ref. [5] were conducted slightly differently. First, the Josephson system was a small-inductance β_L interferometer, which we can conveniently approximate with a single Josephson junction, since the dynamics for small β_L is known to be well represented by a single degree of freedom [23]. Second, the probe pulse was in this case a "dc" pulse as sketched in Figure 1, and the measurements were presented for fixed microwave amplitude and variable duration. We will here provide simulations of the classical system described in Equation (1) and parameterized by information provided in Ref. [5]. Characteristic current and frequency are $I_c = 6.056\mu A$ and $\omega_0 \approx 110 \cdot 10^9 s^{-1}$, which lead to a normalized temperature of $kT/H_J \approx 2 \cdot 10^{-4}$ ($T = 30mK$), and a normalized microwave frequency $\omega_s = 0.6527147$, which is close to the resonance such that $\eta = \sqrt{1 - \omega_s^2}$. We have estimated the dissipation parameter α from the reported decay of Rabi-oscillations, $\alpha = 0.00151477$. The normalized applied microwave amplitude ε_s is varied between 0 and 0.01, and the normalized duration is in the range $[0; 3000]$. Simulations are conducted with

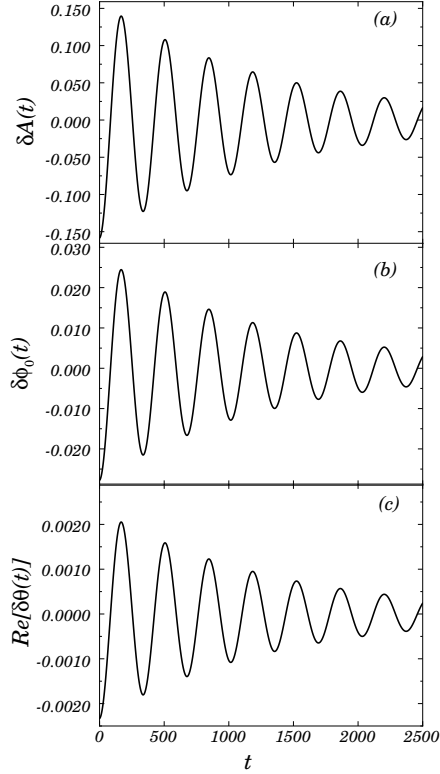


FIG. 4: Linear transient responses to microwave onset versus normalized time as calculated from Equations (28)-(30) for the parameter values of Figure 3.

a probe pulse $\varepsilon_p(t)$ as shown in Figure 1, followed by a short time in which we determine whether or not the junction has switched from the zero-voltage state. For every specific set of parameters, this type of simulation is conducted 25,000 times, each with a randomly chosen value of microwave phase θ_s , and the switching probability is recorded, before a new microwave duration is chosen. Typical results are displayed in Figure 7a, where the switching probability P , reported as population occupancy of excited quantum state in Ref. [5], is shown as a function of microwave duration. We clearly observe the Rabi-type oscillations of this classical system with a distinct frequency. Moreover, the oscillation frequency is in near perfect agreement with the reported comparable figure of the experimental measurements as well as the theoretical value Ω_R provided by the analysis in the above section. Figure 7b shows the simulated system energy as an average of many thermal realizations, each with a randomly chosen θ_s , of the trajectory (at $T \approx 30mK$). The different choices of $\theta_s \in [-\pi; \pi]$ yield slightly different trajectories of $\delta A(t)$, $\delta\theta(t)$, and $\delta\varphi_0(t)$, which in turn make possible switching a function of θ_s . The importance of this ensemble average can be viewed in

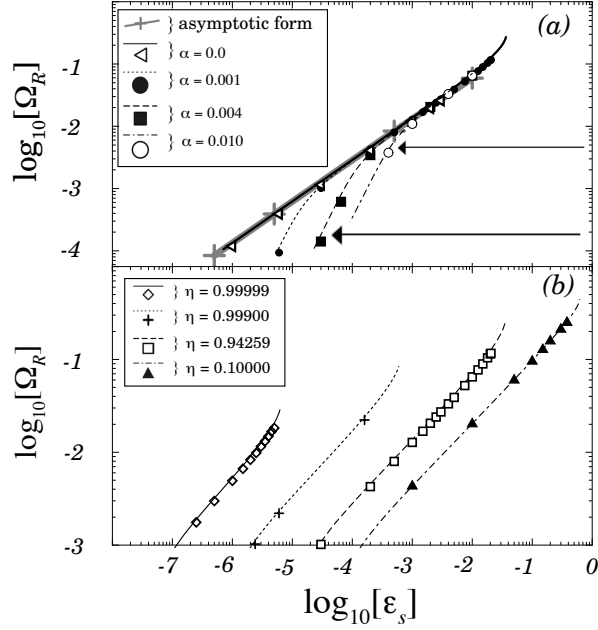


FIG. 5: Normalized modulation frequency Ω_R (at $T = 0$) as a function of normalized signal amplitude ε_s for (a) a range of damping α values, with $\eta = 0.94259$ ($\omega_s = \sqrt[4]{1 - \eta^2} = 0.577886$). Gray line with large "+" markers indicates the asymptotic form given in Equation (27). Arrows indicate the frequency for which small oscillations would be overdamped for respective values of α . (b) A range of dc bias η values, with $\alpha = 0.001$. Curves represent solutions to Equation (17). Markers represent data from numerical simulations of Equation (1) with $\varepsilon_p(t) = T = 0$.

Figure 7c, where a single trajectory of energy is shown for the applied temperature of $T = 30mK$. After a short transient, the thermal effects are dominating the individual trajectory, exciting the modulation frequency Ω_R at random phase. Only after an appropriate average over trajectories do we observe the smoothly decaying envelope of the modulated energy curve in Figure 7b, which in turn is very similar to the (single) zero-temperature trajectory seen in Figure 7d. The close connection between the transient energy modulation and the Rabi-type modulation is obvious, and the close relationship between classical numerical simulations, classical theory, and the experimental measurements is further emphasized in Figure 8, where the experimental data (open markers) of Ref. [5] are shown alongside theory (solid curve) and simulations (closed markers). The three-way close agreement indicates that much about these measurements can be understood from classical theory of driven,

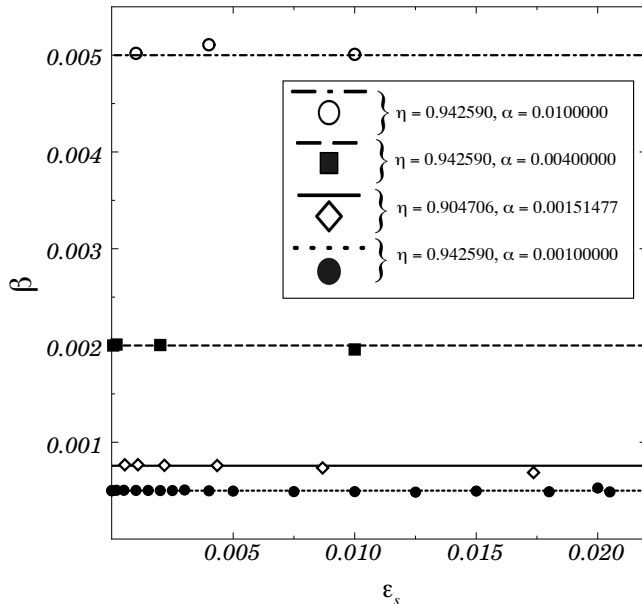


FIG. 6: Normalized attenuation β as a function of damping α and normalized signal amplitude ε_s for $T = 0$. Lines represent the derived relationship $\beta = \alpha/2$ and markers represent data from the simulations of Figure 5.

damped Josephson junctions.

VI. CONCLUSION

We have presented a perturbation analysis of the classical, nonlinear model describing the microwave-perturbed Josephson junction. Results show direct quantitative analogy between experimentally reported Rabi-oscillations and the classical transients to phase-locking, and results are presented as specific functions of experimental system parameters. The analysis in this paper is both a complement and an extension to the analysis of Ref. [17], where an energy balance perturbation approach was applied to produce similar connection between reports of Rabi-oscillations and the nonlinear classical Josephson system. The extension provides direct closed form solutions of a (Rabi-type) modulation frequency as well as attenuation, and the resulting frequency agrees closely with the previously obtained result. This consistency lends credibility to the value of a classical interpretation of the reported Rabi-oscillations, since the quantum mechanical and classical intuition turns out to be very similar (as is also the

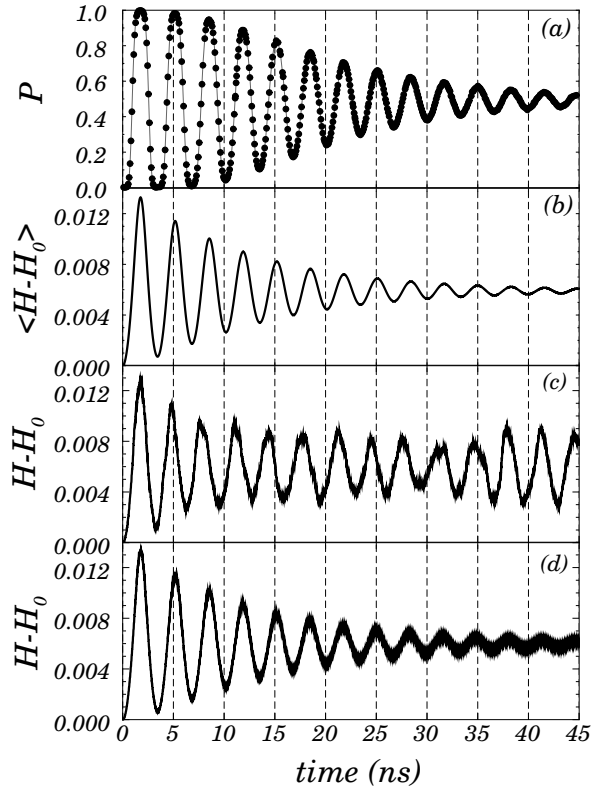


FIG. 7: (a) Escape probability P as a function of signal duration $\Delta t_s \omega_0^{-1}$. Numerically simulated quantities are represented by dots (each of which represents 25,000 escape events). (b) Ensemble average of normalized energy, simulated through Equation (1), as a function of signal duration (ensemble size $N = 50,000$, randomly chosen θ_s). Parameters are: $T = 30$ mK, $\alpha = 0.00151477$, $\eta = \sqrt{1 - \omega_s^4} = 0.904706$, $\omega_s = 2\pi\nu_{01}/\omega_0 = 0.652714$, $\varepsilon_s = 0.00217000$, $\varepsilon_p = 0.0847400$, and $\omega_0 \approx 110 \cdot 10^9 s^{-1}$. These parameters are inspired by those reported in Ref. [5]. (c) Single trajectory of normalized energy versus time for parameters listed for (b). (d) Single trajectory of normalized energy versus time for $T = 0$.

case in laser physics [24]).

The macroscopic quantum picture interprets the observed oscillations as a result of a microwave induced temporal variation in the population probability of two, or more, intrinsic quantum mechanical energy levels in the Josephson washboard potential. This slow variation is then indirectly observed through the associated variation in tunneling probability, switching from the zero-voltage state as a result of the application of the probe pulse. The stochastic nature of the system is due to the absorption of microwave photons as well as the

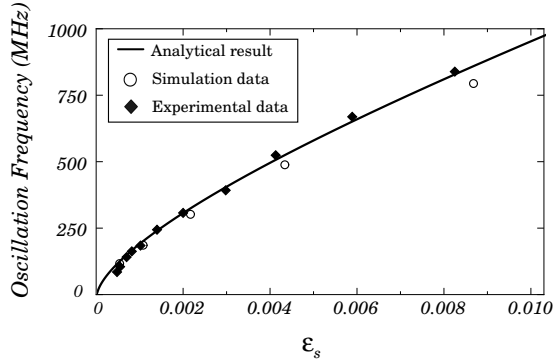


FIG. 8: Modulation frequency Ω_R as a function of normalized signal amplitude ϵ_s for $\alpha = 0.00151477$, $\eta = 0.904706$, $T = 30$ mK. Lines represent calculations using Equation (17), \circ represent statistical data from simulations, and \bullet are the measurements copied from Ref. [5].

subsequent tunneling probability of the measurement.

The classical picture presents a system with a microwave induced temporally modulated energy. The slow variation is indirectly observed through the associated variation in escape from the energy well when the probe is applied, with high probability for passing the energetic saddle point during times of elevated energy and relatively little escape probability during times of depressed energy content. The stochastic nature of this system is due to the random phase of the microwave signal as well as the thermal fluctuations.

Additional analogies between intrinsic quantum mechanical energy levels and the multi-valued resonances of the classical nonlinear system briefly outlined above (as well as in Ref. [17]) further bridges the gap between what can be expected from the two interpretations of the microwave induced measurements. Since the experimental measurements are concerned only with detecting the escape event, and since the classical and quantum mechanical interpretations seem to provide the same signatures for that escape, we are faced with a fundamental ambiguity of how to read this information. Potential applications of Josephson technology for quantum information processing will therefore benefit from the development of new unambiguous measurements, which must present signatures of macroscopic quantum behavior that cannot be explained classically. However, we submit that, given the very close quantitative agreement between our classical theory and the experimental measurements, the intuition and the closed form expressions presented in this paper can be directly applied to guide future experiments and microwave manipulations of Josephson systems.

VII. ACKNOWLEDGMENTS

This work was supported in part by the UC Davis Center for Digital Security under AFOSR grant FA9550-04-1-0171 and in part by MIUR (Italy) COFIN04.

- [1] I. I. Rabi, Phys. Rev. **51**, 652 (1937).
- [2] J. M. Martinis, S. Nam, and J. Aumentado, Phys. Rev. Lett. **89**, 117901 (2002).
- [3] A. J. Berkley, H. Xu, M. A. Gubrud, R. C. Ramos, J. R. Anderson, C. J. Lobb, and F. C. Wellstood, Phys. Rev. B **68**, 060502 (2003).
- [4] R. W. Simmonds, K. M. Lang, D. A. Hite, S. Nam, D. P. Pappas, and John M. Martinis, Phys. Rev. Lett. **93**, 077003 (2004).
- [5] J. Claudon, F. Balestro, F. W. J. Hekking, and O. Buisson, Phys. Rev. Lett. **93**, 187003 (2004).
- [6] A. O. Caldeira and A. J. Leggett, Phys. Rev. Lett. **46**, 211 (1981).
- [7] *Quantum Computing and Quantum Bits in Mesoscopic Systems*, A. Leggett, B. Ruggiero, and P. Silvestrini Eds. (Kluwer Academic/Plenum Publishers, New York, 2004).
- [8] J. M. Martinis, M. H. Devoret, J. Clarke, Phys. Rev. Lett. **55**, 1543 (1985).
- [9] J. R. Friedman, V. Patel, W. Chen, S. K. Tolpygo, and J. E. Lukens, NATURE (London) **406**, 43 (2000).
- [10] A. Wallraff, T. Duty, A. Lukashenko, and A. V. Ustinov, Phys. Rev. Lett. **90**, 037003 (2003).
- [11] A. Wallraff, A. Lukashenko, J. Lisenfeld, A. Kemp, M. V. Fistul, Y. Koval, and A. V. Ustinov, NATURE (London) **425**, 155 (2003).
- [12] N. Grønbech-Jensen, M. G. Castellano, F. Chiarello, M. Cirillo, C. Cosmelli, L. V. Filippenko, R. Russo, and G. Torrioli, Phys. Rev. Lett. **93**, 107002 (2004).
- [13] N. Grønbech-Jensen, M. G. Castellano, F. Chiarello, M. Cirillo, C. Cosmelli, V. Merlo, R. Russo, and G. Torrioli, in "Quantum Computing: Solid State Systems", edited by B. Ruggiero, P. Delsing, C. Granata, Y. Paskin, and P. Silvestrini (Kluwer Academic and Springer Publishers, New York, in press), cond-mat/0412692.
- [14] N. Grønbech-Jensen and M. Cirillo, Phys. Rev. B **70**, 214507 (2004).
- [15] M. Cirillo, P. Carelli, M.G. Castellano, F. Chiarello, C. Cosmelli, N. Grønbech-Jensen,

- R. Leoni, J.E. Marchese, F. Mattioli, D. Simeone, and G. Torrioli, accepted for publication in *Physica C* (2005).
- [16] P. S. Lomdahl and M.R. Samuelsen, *Phys. Lett. A* **128**, 427 (1988); N. Grønbech-Jensen, Y. N. Kivshar, and M. R. Samuelsen, *Phys. Rev. B* **47**, 5013 (1993).
- [17] N. Grønbech-Jensen and M. Cirillo, *Phys. Rev. Lett.* **95**, 067001 (2005).
- [18] A. Barone and G. Paternó, *Physics and Applications of the Josephson Effect* (Wiley, New York, 1982); T. Van Duzer and C. W. Turner, *Principles of Superconductive Devices and Circuits*, 2nd ed.(Prentice-Hall, New York, 1998).
- [19] G. Parisi, *Statistical Field Theory* (Addison-Wesley, Redding, MA, 1988).
- [20] N. F. Pedersen, M. R. Samuelsen, and K. Saermark, *J. Appl. Phys.* **44**, 5120 (1973).
- [21] See, e.g., I. S. Gradshteyn and I. M. Ryzhik, *Table of Integrals, Series, and Products*, 4th Ed. Academic Press, Inc (1979).
- [22] This simple expression is not sensitive to the microwave phase θ_s , which does have some influence on the transient oscillations (to be published).
- [23] N. Grønbech-Jensen, D. B. Thompson, M. Cirillo, and C. Cosmelli, *Phys. Rev. B* **67**, 224505 (2003).
- [24] Y. Zhu, D. J. Gauthier, S. E. Morin, Q. Wu, H. J. Caramichael, and T. W. Mossberg, *Phys. Rev. Lett.* **64**, 2499 (1990).